

RESEARCH ARTICLE

Performance Analysis of Cobalt Chromium Alloy Based Femoral Knee Components Polishing Using Industrial IRB 2400 Robot

Vasanth kumar.CH¹ | M Uma² | M.M. Reddy³ | Ragavendra Rao.V⁴ | Prabhu Sethuramalingam⁴ 

¹Department of EIE (SCOFT) Saveetha Engineering College, Chennai, India | ²Department of Computational Intelligence, SRM Institute of Science and Technology (KTR), SRM Institute of Science and Technology, Kattankulathur, Chennai, India | ³Department of Mechanical Engineering, Curtin University, Miri, Malaysia | ⁴Department of Mechanical Engineering, SRM Institute of Science and Technology, Kattankulathur, Chennai, India

Correspondence: Prabhu Sethuramalingam (prabhus@srmist.edu.in)

Received: 26 February 2025 | **Revised:** 26 April 2025 | **Accepted:** 6 July 2025

Funding: The authors received no specific funding for this work.

Keywords: Cobalt chromium alloy | depth first search algorithm | IRB 2400 Industrial Robot | polishing | robot kinematics | surface roughness | Trizact belts

ABSTRACT

The research aims to study the surface characteristics analysis of cobalt-chromium alloy which is mostly used in femoral knee components using Industrial IRB 2400 Robot. Initially manual polishing from basic SiC abrasive papers to diamond slurry with a cloth polishing to achieve N2 grade of super finishing surfaces by the 11-step process. For incorporating the observation to polish the curved surface workpiece, the curve fit method is used by projecting its surface's curves on 2D planes, and thus, data on several control points for each continuous curve is obtained which gives a uniform polishing. To obtain desired grade of polishing in the least robot cycle time, 3 M Trizact belts of P1200 and P2500 equivalent grades as used for 1st two polishing stations of the Robot Finishing Cell. An industrial robot manipulator IRB2400 is used for polishing the workpiece to N2 grade. Forward kinematics helps in deciding the best use of the robot's work cell and inverse kinematics is calculated for avoiding singularities. After incorporating the data of several control points into the Depth First Search algorithm of robot programming. Surface finish results are explained using experimental observations which address the achievement of N2 super-finishing of the femoral knee component surfaces.

1 | Introduction

Before implanting any prosthetic component in a human body, a study of its surface roughness should be done to avoid natural problems like body fluid clotting inside the cavity of the surface, uneven growth of tissues inside the cavity of the surface, a degree of freedom of biomechanical motions tending to rigidity due to uneven surface roughness. Industrial robot board has different properties which cover physical as well as electrical aspects which are needed to be considered for its selection for the required surface finish on the implant. Secondly, during the selection of the robot, its Ingress Protection (IP) grade

should be considered which tells about the environment in which the robot can sustain. For polishing any component, the robot should be dust compatible and if any fluid is used for super finishing, the robot should be liquid compatible also. According to ABB robot manufacturers, IP68 is a protective robot for polishing purposes (<http://new.abb.com/low-voltage/products/conduit-fittings/adaptaflex/news/applying-ip-ratings-to-flexible-conduit>) i.e., it is protected from dust and also protected against a long period of immersion in water. But for polishing purposes, IP54 is best suited because it resists solid dust deposition on it and also protects itself from a high jet of water spray from any direction into the cell.

Industrial robots are used for heavy and fine repeatability properties which are useful for different batches and mass production of different components. Polishing any component requires the fineness of grains on it which indicated the larger grain density of the surface (Brunetter et al. 2001). Polishing robots are programmed to apply sufficient pressure on the surface of the component during polishing. Secondly, it is also desired to have precise movement in the right direction and it is all possible because of a well-selected robot. While polishing, it is also needed to improve the total cycle time with minimum waste. On the other hand, it is very important to save human damage during polishing operations. Hence, for overcoming these problems, a well-selected robot is brought into action.

Different metal alloys used in orthopedic implants should be studied for their structural and mechanical properties before implanting. They observed that there is a damage pattern known as inflammatory cell-induced (ICI) corrosion (Gregory et al. 2017). This corrosion is due to bone self-recovery and deposition of grown bone in the corrosive area of the implanted metal. To overcome this problem, they suggested using a super finish surface of the implanting metal so that due to the high density of surface grains, the problem of ICI corrosion was solved. The selection of materials should be characterized by their structural properties, implant design, and manufacturing regularities. Traditional materials for the implants are stainless steel, cobalt alloys, titanium alloys, etc. These materials are consistently being modified and improved on their surface finish aspect and structural design (Jones et al. 2017).

Explaining fretting corrosion in the implants inside the human body (Hallab 2017). They explained fretting corrosion comes with relative micro motions between the metal of the implant and the natural bone. This corrosion leads to the formation oxides layer on the metal of the implants resulting in resistance in the motion of the respective component. The notations and technical names for the implant components are, Femoral, which is the largest bone of the body. The condyle is the artificial supporting knee to the femur (Jones et al. 2017). The femoral condyle is a critical component of knee joint prostheses, typically fabricated using high-strength biomaterials such as cobalt-chromium or titanium alloys. These materials are selected for their wear resistance, biocompatibility, and ability to withstand mechanical loads experienced in total joint arthroplasty procedures. There is no standard treatment for repairing the femoral part of the body which finally leads to artificial implants (Ebrahim et al. 2012). After experimenting on different implant types to replace the natural, it was tested with different types of loadings. The maximum load given was 3000 N. The slope of the femur was changed after some cycles of loads. Hence it is a very essential part of the treatment to replace the femur with an artificial femoral Condyle. Super-finishing the surface of the femur can withstand the stress cycle. Resurfacing the femur surface can increase the toughness and hardness of the femur and can resist femoral neck fracture (Little et al. 2007).

Compressive properties of the femur were studied and concluded that after axial loading, the strain rate of the femur comes out to be 0.002, 0.1, and 9.16 per sec after incremental loadings. Making super finishing of the Condyle surface, the

yield point gets shifted to the upside to stress direction according to hooks law (Ducheyne et al. 1977). Different load conditions were given to the femur bone to calculate the strain at different nodes. The nodes bending were evaluated using bending moment. The experiment was done by reducing the length of the femur comparatively if the stain with a shorter length can be improved (Arno et al. 2012). The modern design of the prosthetic components includes the combination of curves which decreases the constraints on the motion of the femur (Crocklarell et al. 2010). Some aspects as material selection and structural properties like hardness are considered to be relieving the pain in the joint function of the patient (Tigani et al. 2013).

Biomaterials that would not react to the tissues should be chosen or should be coated according to the material adhesiveness (Zhenyu and Jukka Pajarinen 2015). Those materials are helpful in orthopedic surgery. For example, Titanium alloy is very reactive to muscle tissue and can make decompose the tissues. Alumina coating is a commercial practice to avoid such problems. A review of the wear mechanisms has been carried out whose primary cause the premature failure due to wearing of the implants. Material Design comes with safe tensile and transverse loads on the implants (Buford and Goswami 2004). Dimensions of the implants play a very important role in the same. Topological overview of the small implants are studied and described that the resurfacing of the implants till super finishing can increase the life cycle of the implant (Byran et al. 2012).

2 | Proposed methodology

The proposed methodology as shown in Figure 1 includes the standards of surface representation and surface measurement techniques. Steps of experimentation include developing proof of concept on flat material samples and coupon-level polishing before using the robot for the same. After each experiment, the surface roughness was again measured as per the method studied from the standards of surface engineering. The desired material of the component which is to be polished is Co-Cr. Following this desirable condition, some steps are taken for evaluating proof of concept by polishing a flat piece of Co-Cr by rubbing its surface on premium SiC abrasives paper manually which is referred to as coupon level polishing (Zaman et al. 2017). That is without using the robot. This procedure is done to validate that the desired material can reach N2 (0.02 microns) and if it can, in how many steps and in how many several strokes. After validating the POC, a Robot Finishing Cell RFC is designed with the corresponding positions of the polishing machines according to robot cell design standards. RFC is designed with the help of component selections which are going to be implemented into the cell and have important significance on the polishing process. The cell includes the robot ABB IRB 2400, femoral Condyle Robot fixture, polishing stations, and robot programming. The femoral Condyle section is followed with a curve fit approach to extract mathematical information about the workpiece and implement the data into robot programming which is made with the support of the forward and inverse kinematics of the robot.

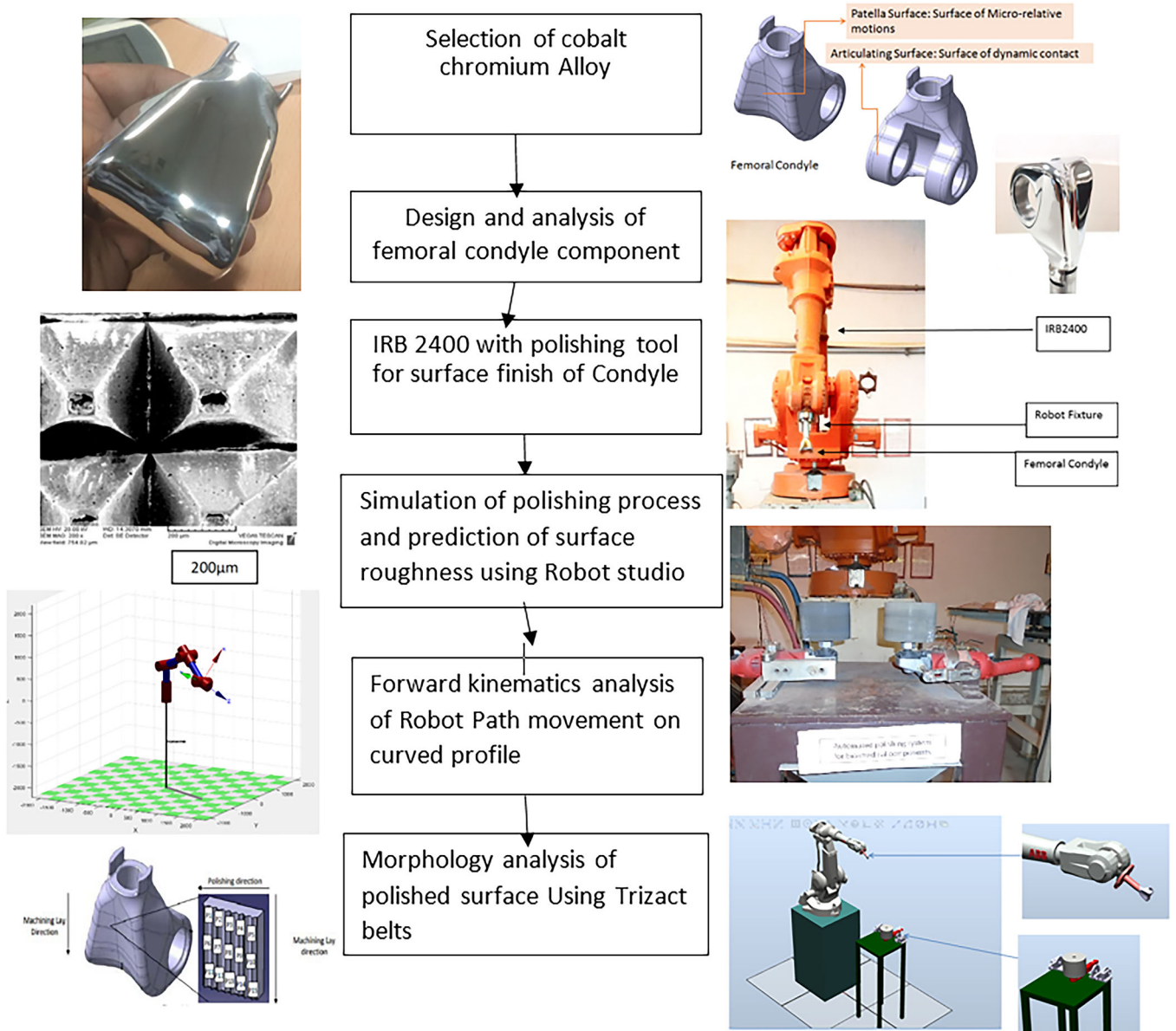


FIGURE 1 | Proposed methodology. [Color figure can be viewed at wileyonlinelibrary.com]

3 | Experimental Design and Analysis

Cobalt–chromium–molybdenum (Co–Cr–Mo) alloys are widely used for removable partial dentures, and metal frames, because the alloys are strong and resistant to corrosion. These alloys have also been used for bone fixation devices and total hip and knee replacements in orthopedics in both the cast and wrought forms, and Co–Cr–Mo alloys are now essential for medical applications (Arun and Jadhav 2016).

3.1 | Effect of Surface Finish of Cobalt-Chromium Alloy Using IRB2400 Robot Polishing Process

Figure 2 depicts the different stages of the robot polishing process. In the first stage, the belt chosen is Trizact A16 (European standard: P1200), which has the highest roughness among all the belts. This belt has comparatively more material removal ability. As a result, during polishing on

this belt, the pressure applied by the robot should be minimal. This belt gives the roughness value of the surface to 0.3 – 0.2 μm . In the 2nd stage, the belt chosen is Trizact A6 (European standard: P2500), which has lower roughness as compared to A16. This belt has comparatively less material removal ability. As a result, during polishing on this belt, the pressure applied by the robot should be moderate. This belt gives the roughness value of the surface to 0.07–0.06 μm . After the 2nd stage, the surface is treated with diamond slurry. This helps the surface to get cooled at a higher stage, and the diamond particle, which is present inside the slurry, fills the spaces between the peaks and valleys of the surface. As a result, when treated on the compressed cotton cloth unbounded wheel, the sully then removes the micron-thin layer of the surface. In the third stage, the slurry removes some material from the surface, and as the wheel is of cotton material, the removed particles get stuck to the cotton cloth surface, and because of the recurring surface of contact with the wheel, the particles thus restrict the surface to get the super finish. 0.05–0.03 μm . The fourth stage is

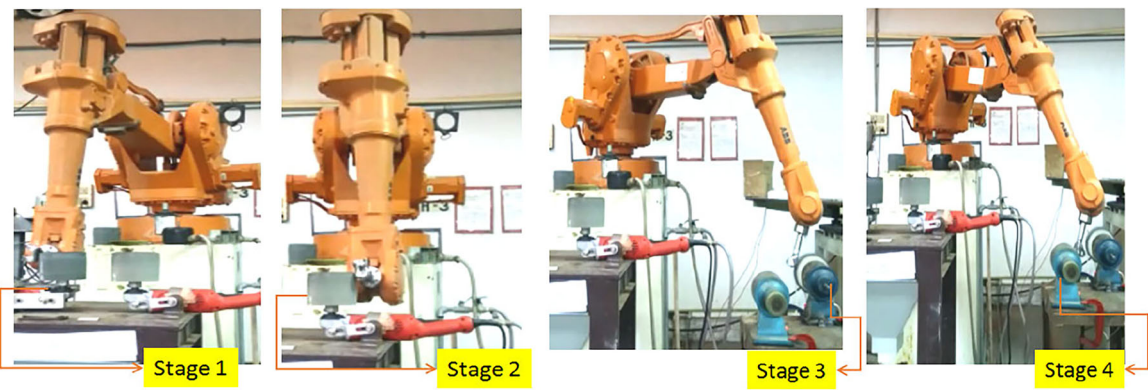


FIGURE 2 | Experimental setup of IRB2400 Robot having polishing tool with different stages. [Color figure can be viewed at wileyonlinelibrary.com]

the proceeding stage of stage 3 where the surface will be treated without a diamond slurry. At this stage, the surface will be thus get free from unwanted removed material, and hence, the surface reaches the super finishing scale 0.02–0.008 μm (Kandlikar et al. 2005).

4 | Results and Discussions

4.1 | Computational Forward and Inverse Kinematic Analysis of Robot Polishing Tool

According to the Denavit Hartenberg(DH) criterion for calculating the kinematics of a robot, the primary thing to do is to evaluate DH parameters, which are shown in matrix Equation (1). These parameters are incorporated together in a homogeneous transformation matrix, which contains data on link rotation and link transformation. Below shown is the matrix formulation of an arbitrary single link.

$$A_i(q_i) = \begin{bmatrix} \cos \theta_i & -\sin \theta_i \cdot \cos \alpha_i & \sin \theta_i \cdot \sin \alpha_i & a_i \cdot \cos \theta_i \\ \sin \theta_i & \cos \theta_i \cdot \cos \alpha_i & -\cos \theta_i \cdot \sin \alpha_i & a_i \cdot \sin \theta_i \\ 0 & \sin \alpha_i & \cos \alpha_i & d_i \\ 0 & 0 & 0 & 1 \end{bmatrix} \quad (1)$$

Where i is the number assigned to the link, i-1 is the previous link, and the matrix is the position of link i concerning i-1, and q_i is the element numbering of the link (Arun and Jadhav 2016). Hence, for every link, this DH matrix is made, and for the net pose of the robot, the last link is the product of all DH matrixes of the links, and that is known as the homogeneous transformation matrix of the robot. All DH matrix for links 1 to 6 are shown below:

Let $q_1 = q_2 = q_3 = q_4 = q_5 = q_6 = 0$ degrees. That is, all he links are at 0 degrees twist.

Now, the homogeneous transformation matrix of the robot will be,

$$A_{06} = (A_{01})(A_{12})(A_{23})(A_{34})(A_{45})(A_{56})$$

$$A_{06} = \begin{bmatrix} 1 & 0 & 0 & 840 \\ 0 & -1 & 0 & 0 \\ 0 & 0 & -1 & -140 \\ 0 & 0 & 0 & 1 \end{bmatrix} \quad (2)$$

Below shown is the 3D representation of IRB2400 using Peter Corke's robot toolbox in MATLAB using homogeneous transformation matrix A06.

The robot IRB2400 has represented position P (840, 0, -140) with x, y, and z directions respectively. Knowing all the directions of the robot, it is easy to program the robot offline as well as in online mode. The Figure 3 shows the direction of x, y, and z, which is the real-time orientation of the robot when it is in the home position. Now, for experimentation, if the robot is desired to move as $q_1 = -25^\circ = q_2 = q_3$, $q_4 = -15^\circ$, $q_5 = -23^\circ$, and $q_6 = -15^\circ$. Therefore, the homogeneous transformation matrix for the orientations input from above values will be as follows

$$A_{06} = \begin{bmatrix} 0.4022 & -0.1588 & 0.9017 & 1214 \\ 0.3422 & -0.8874 & -0.3089 & -566.2 \\ 0.8492 & 0.4328 & -0.3026 & 484.7 \\ 0 & 0 & 0 & 1 \end{bmatrix} \quad (3)$$

Inverse kinematics is just the opposite direction calculation in robot kinematics. It is the evaluation of joint parameters that is the angle of twists w.r.t to link parameters that are the pose of the link. To solve for the solutions for each joint parameter that is the angle of twists of the links, inverse kinematics identities proposed by John Craig are used (Arun and Jadhav 2016). Hence, there are 6 sets of solutions because there are 6 revolute joints of IRB2400, and hence, 6 joint parameters. The solution is proposed below, let for the calculation it is needed the robot's TCP is to reach P (1142, 0, -148) = P (Px, Py, Pz). Major positional joint parameters are only above three angles by which the TCP of the robot moves for major displacements. The rest of three angles are the wrist position of links 4, 5, and 6 of IRB2400. These parameters are determined with the dependencies of the above three angles and their corresponding DH matrix. Hence, for further calculation, the DH matrix of the major 3 links is made using all the above three angles and assuming the wrist angles be zero.

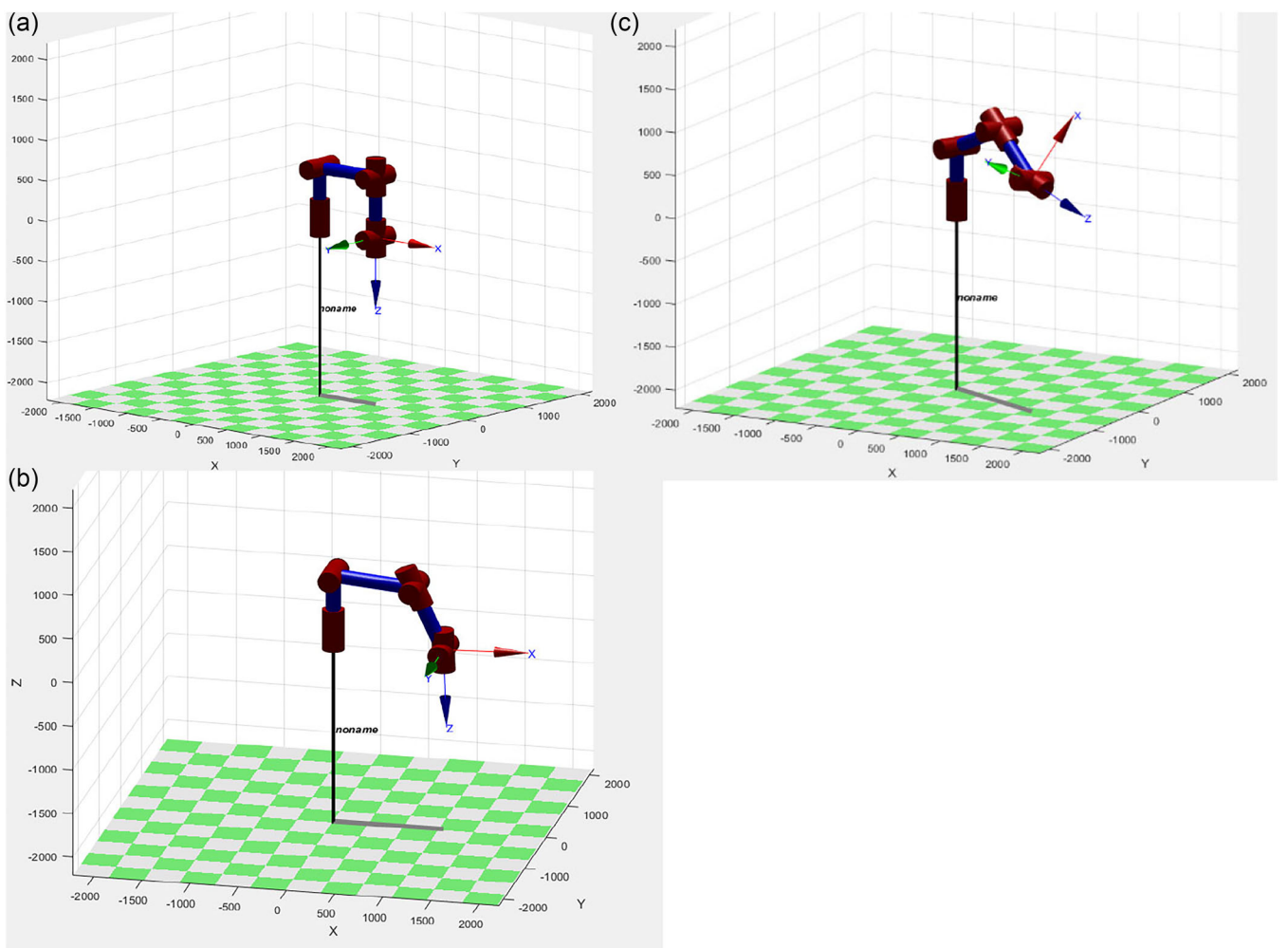


FIGURE 3 | 3D positional representation of polishing tool of IRB2400 robot (a) Home position (b) Forward kinematic position (c) Inverse kinematic position. [Color figure can be viewed at wileyonlinelibrary.com]

$$A06 = \begin{bmatrix} 0.9993 & 0 & 0.0370 & 1142 \\ 0 & -1 & 0 & 0 \\ 0.0370 & 0 & -0.9993 & -148 \\ 0 & 0 & 0 & 1 \end{bmatrix} \quad (4)$$

Hence, the matrix obtained from the angle evaluated from inverse kinematics satisfies the desirable points Px, Py, and Pz as 1142, 0, -148, respectively. Below shown is the robot link plot on the respective position using Peter Croke toolbox in MATLAB. Inverse kinematics have different solutions for the same point. It's because of the degree of versatility of the robot, which can move to the desired position in different ways and from different directions. Inverse kinematics not having many solutions because the algorithm faces a singularity in the robot while moving from one target position to another target position in optimizable link displacement.

4.2 | Simulation of IRB 2400 Robot for Polishing Cobalt Chromium Alloy

ABB IRB 2400 Robot with 20 kg of holding capacity has a virtual simulation station provided by ABB as Robot Studio. The robot finishing cell is first designed on a virtual platform with real-time dimensions, as the imported geometry

in the robot studio. Both fixed-position components and the moving compounds are being attached to the robot studio platform concerning world-coordinated systems. According to the real-time robot finishing cell setup, the robot is on a platform with a height of 1470 mm above the ground level. Similarly, the bench on which the grinding machine, as the fixed position component, is mounted is of height 1250 mm from the ground. The tool data is defined according to the dimensional property of the fixture and the Condyle. For polishing all nine surfaces of the Condyle, the robot is taught different targets and paths. The important aspect of path planning is to decide the orientation of the robot to approach the target position. The robot studio is already being designed to have pre-saved orientation values for the respective target positions of the robot. The provision for the program is to select the orientation values from the provided GUI of the robot studio. Path planning can be made by predefining the shape of the path in the simulator itself. For this case, the boundaries of the patella surface were extracted from the option provided in the GUI of the simulator. After the boundary selection of the surface, it is projected to the surface of the belt on the grinding machine to follow the same path by the tool center of the robot. Different visuals can also be selected in the simulator to overcome the problem of differentiation of the surfaces.

After all, fixing the tool data point, work object, and path shape, finally, the robot is taught with a designated orientation to reach the target points and men, while the points are saved as the MOVE commands of the ABB Robot RAPID Program syntax into the virtual flex pendant. Figure 4 portrayed the path selection for the robot tool data point of fixed orientation. This path is specifically designed for polishing the patella surface of the femoral Condyle. This path generation explains the availability of free space for the robot in its robot cell for its respective movement.

4.3 | Polishing Process of Femoral Condyle

The femoral Condyle (FC) is the part of the longest bone of the body. Relative motions are seen at the articulating surface of FC, and the Femoral Bone is fitted to the top taper female section of FC, as portrayed in Figure 5 was made in CATIA V20 Software.

The following are the isometric views of FC. FC is an unsymmetrical geometry. The weight of FC is approximately 50 grams. FC was designed with multiple combinations of different types of Bezier and B-spline curves. Each curve has its own set of control points. For the geometric study of FC, the location of these control points in a reference plane was studied, and classified the surfaces of FC were classified according to the continuity of the control points concerning each other.

To overcome the error in morphologically maneuvering TCP during its reorientation during travel from one control point to another, the surfaces are subdivided into different areas to target small elementary surfaces at a time. This approach was made to make the polishing uniform throughout the surface of the Condyle. Below shown is the sun-division of the surface and the corresponding explanations.

Above shown is the subdivision made of surface 9 of the Condyle, and according to these subdivisions, the robot TCP is maneuvered for keeping the surface uniform. Each surface subdivision is added to the next, which is known as overlapping in the polishing process, and due to this overlapping, surface uniformity of the critical surface was achieved. In Figure 5, the subdivisions are shown in brown color code to indicate the active polishing step for the corresponding surface. Subdivision 1 contains 2 edges and an inner arc-making surface which has a critical nature of high deformability due to less area. Hence, this surface is the 1st critical surface that is polished at the slow

speed of the robot to maneuver TCP is a satisfactory covering morphology of the surface. In the next steps, the surfaces are chosen with their corresponding side edges to keep the uniformity of the Condyle. Till step 5, the surface is polished with the overlapping approach with the orthogonal direction of moving TCP w.r.t the machining lay. In Steps 6 and 7, the Condyle is polished by moving TCP at 180 degrees of the machining lay direction to keep the uniformity of the 3D change in curvilinear morphology as portrayed in the figure. As explained, the polishing overlapping is also done in further polishing also as shown in Figure 6.

shown above is the surface chosen for polishing of articulating surface according to the robot's maximum reach on the polishing machine. Shown above is the surface chosen for polishing of side surfaces of the Condyle according to the robot's maximum reach on the polishing machine. On-symmetric subdivision of the surface is done because the nonsymmetric structure of the Condyle itself is seen and hence, at one face, the subdivisions are fewer as compared to the corresponding opposite face. The first challenge while programming the robot manually for polishing the Condyle is to assign several control points for discontinuous surfaces of the Condyle. Manually, for one curve on the surface, about 100 control points can be increased but that is found to be not sufficient enough to cover the surface roughness value to 0.01 microns uniformly. To solve the problem, the robot speed is decreased by 2% and the number of control points is increased by 100 numbers.

4.4 | Analysis of Robot's End Effector

The robot's end effector is a very important component for polishing kind of operations. The selection process of the fixture should be standardized for this type of application. Hence, at the primary stage, the total load was calculated, which includes the load of the Condyle, the pressure that will be applied on the Condyle, and the load of the fixture itself, which in the net did not exceed 10 N of force. At the next stage, while fixing the fixture onto the robot, it will behave like a cantilever beam, and finally, all the bending properties of the cantilever beam are studied. Further, accordingly the diameter of the shaft and the pitch circle diameter according to the robot's 6th link measurements were designed. To keep the fixture away from micro relative movement w.r.t to the robot's 6th link, some provisions were made on the fixture as depicted in Figure 7.

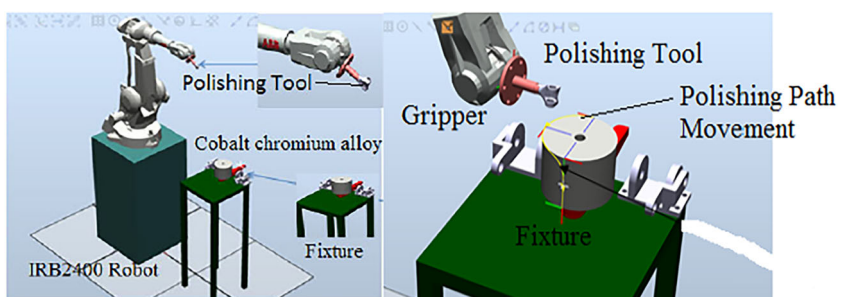


FIGURE 4 | Virual IRB2400 Robot with polishing tool. [Color figure can be viewed at wileyonlinelibrary.com]

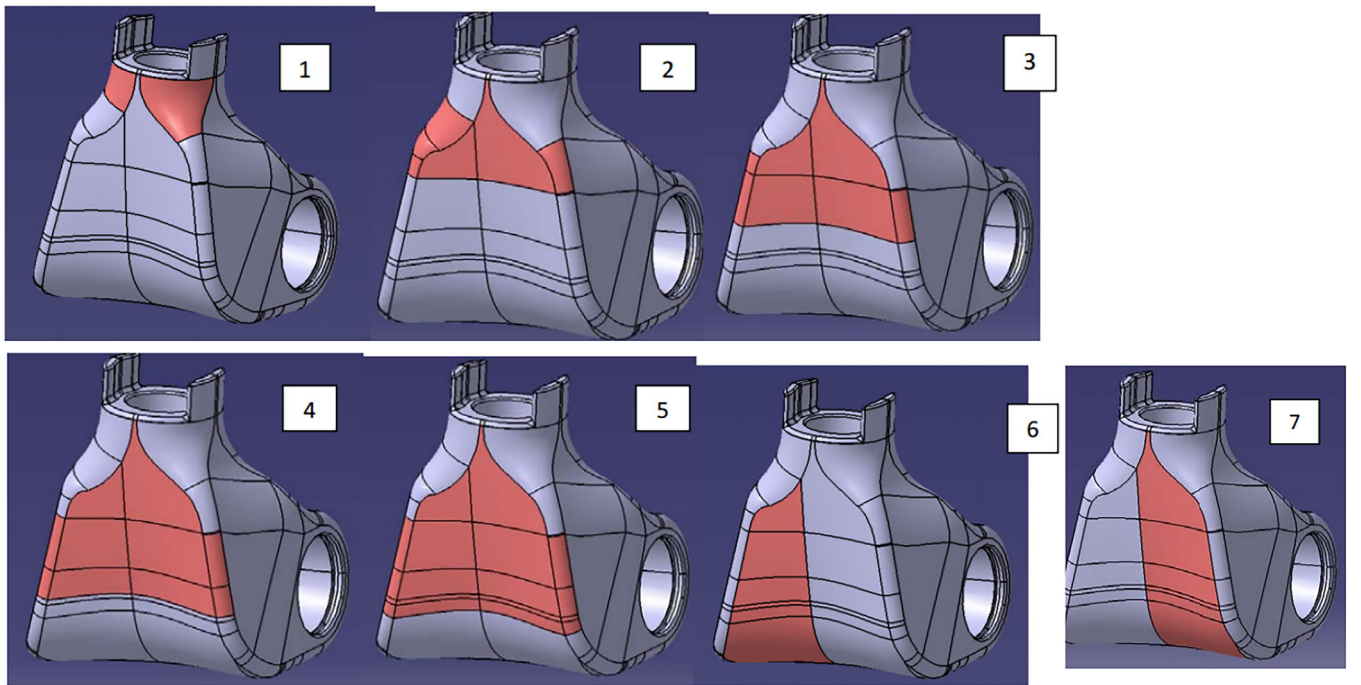


FIGURE 5 | Control points of the surface of the Femoral Condyle. [Color figure can be viewed at wileyonlinelibrary.com]

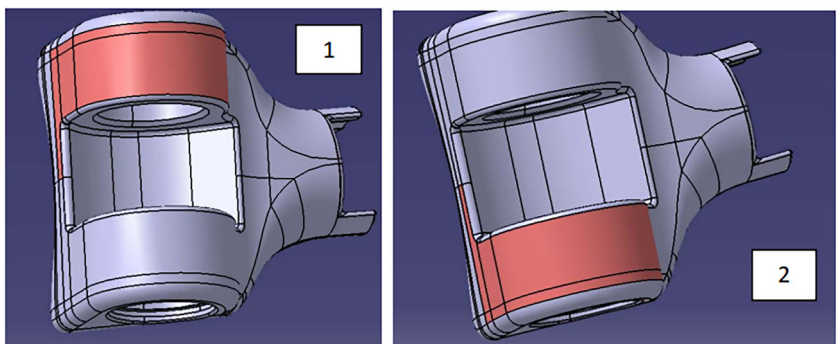


FIGURE 6 | Polishing of the side surfaces of the Condyle. [Color figure can be viewed at wileyonlinelibrary.com]

Bending analysis of the fixture is done using analytically as shown below: Bending moments at fixed end at Section 1 of the cantilever fixture,

$$M = \sum_{1}^3 \frac{(Mn)(Ln)^2}{2E(In)} \quad (5)$$

$$\text{Slop} = \sum_{1}^3 \frac{(P)(Ln)^2}{2E(In)} \quad (6)$$

$$\delta = \sum_{1}^4 \frac{(P)(Ln)^3}{3E(In)} \quad (7)$$

Where, D = Diameter of the shaft, L = Length of the shaft, P = Load, E = Modulus of elasticity = 68.9 GPa, I = Moment of inertia = $\sum_{1}^4 \frac{\pi}{64} (Dn)^4 = 9616.8 \text{ m}^4$, Hence, total deflection in the cantilever beam will be, Deflection = (M) + (Slop) + (δ) Hence, from Equations (5–6) can get the deflection of end effector is depicted in Figure 8.

The above deflection calculation is done with reference to Aluminum material with 68.9 GPa modulus of elasticity.

4.5 | Effect of Robot Polishing Process on Cobalt Chromium Alloy

Before programming the robot, the robot needs to be calibrated according to the given frame of reference as depicted in Figure 9. The calibrated point of the robot is taken as the home position of the robot and the orientation changes will be calculated concerning the calibrated position. Inside the Teach pendant of IRC 5, an option of calibration is made in which the mode updates the position of the home position of the robot, and if needed, the position is made routine in the program to bring the robot to the calibrated home position after the full program is been executed. The depth-first search algorithm is applied for acquiring the primary task of the optimized total cycle time of the polishing cycle by the robot. In search algorithms, the points on the surface will represent the nodes of the search tree, and the lowest distance will be its forward search in the tree. In robot path planning, these points are considered on the surface of the Condyle, and using the algorithm, the Tool centre point (TCP) point of the robot is moved. DFS (Depth-first search algorithm) keeps walking down a path until it is forced

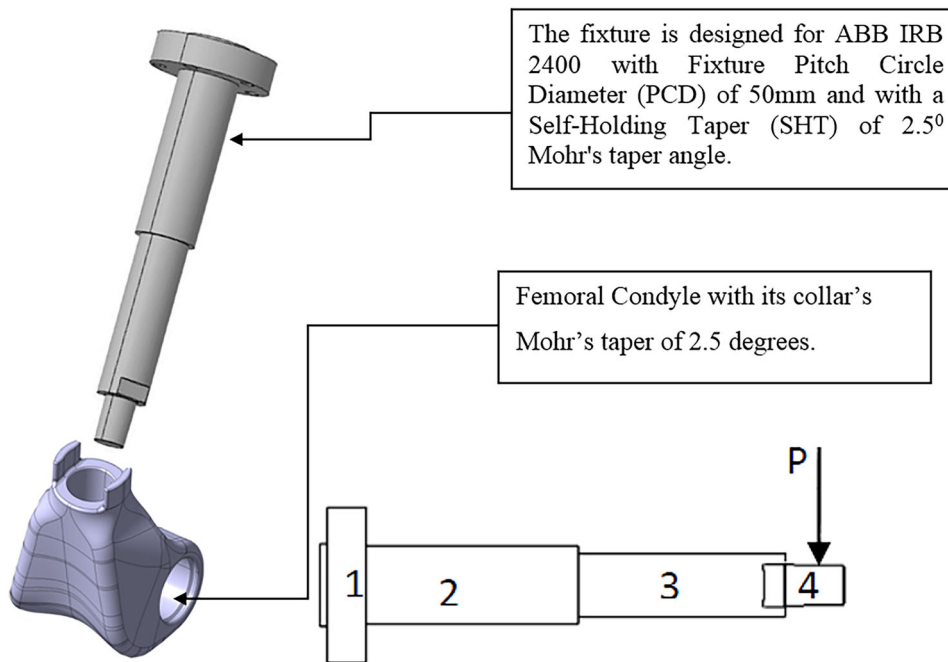


FIGURE 7 | Design of polishing tool end effector. [Color figure can be viewed at [wileyonlinelibrary.com](https://onlinelibrary.wiley.com)]

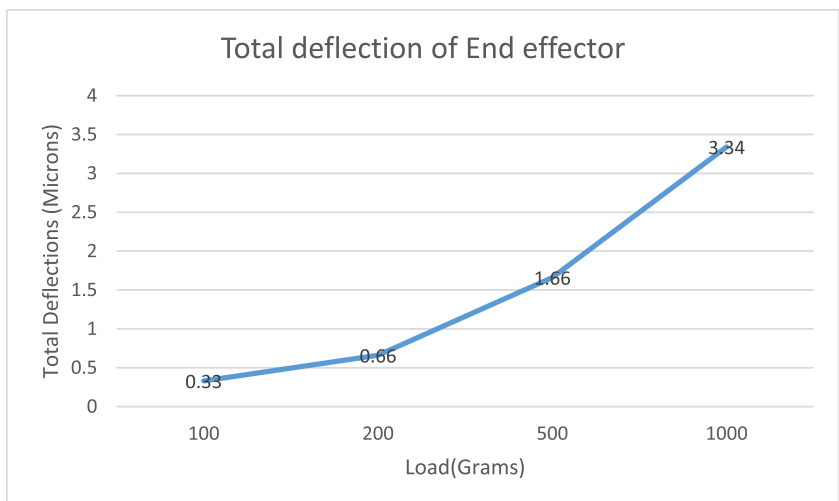


FIGURE 8 | Total deflections of polishing tool end effector. [Color figure can be viewed at [wileyonlinelibrary.com](https://onlinelibrary.wiley.com)]

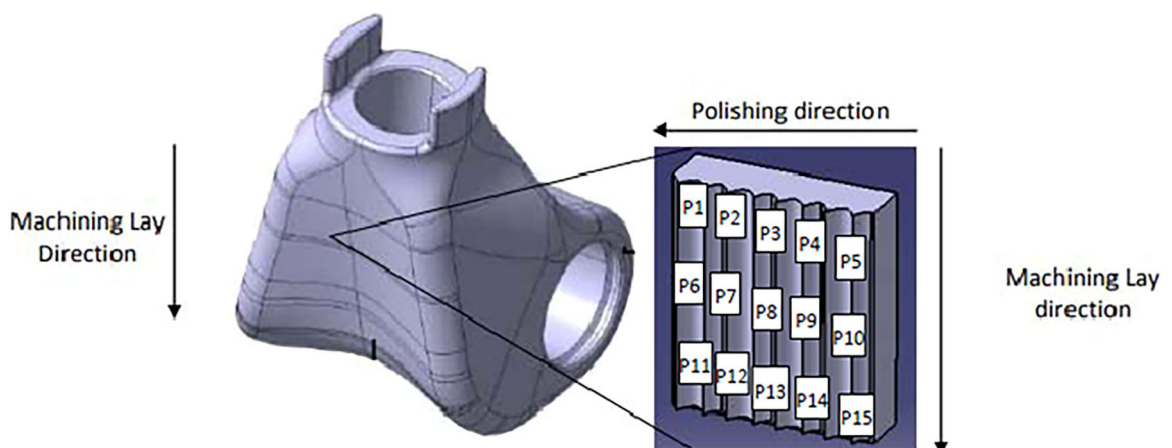


FIGURE 9 | Surface of femoral condyle using depth first search method. [Color figure can be viewed at [wileyonlinelibrary.com](https://onlinelibrary.wiley.com)]

to backtrack. It backtracks until it finds a new path to go down. It results in a search tree, called the depth-first search tree as portrayed in Figure 10.

4.5.1 | Algorithm: Depth First Search (DFS)

1. If the initial state is a goal state, quit and return to success.
2. Otherwise, loop until success or failure is signaled.
 - (a) Generate a state, say A, and let it be the successor of the initial state. If there is no successor, signal failure.
 - (b) Call Depth-First Search with A as the initial state.
 - (c) If success is returned, signal success. Otherwise, continue in this loop.

This recursive nature of DFS can be implemented using stacks as mentioned in Table 1. The idea is as follows: Pick a starting node and push all its adjacent nodes into a stack. Pop a node from the stack to select the next node to visit, and push all its adjacent nodes into a stack. Repeat this process until the stack is empty. Ensure that the nodes that are visited are marked. This will prevent you from visiting the same node more than once.

4.6 | Control Points on Femoral Condyle

Three projections on different planes are taken to determine the control points of the curves concerning the coordinates of the respective plane. The curves are distributed into intervals according to their point continuity, and then made the curve fitting for the respective distributed curve sections. Following are the projection figures (Figure 11) made from CATIA V5 R20.

For uniform polishing of any component, it's very important to apply uniform pressure along the surface. Curve fitting is the approach used for determining the domain of continuity and discontinuity of the curves on the surface, which will help in determining the number of control points needed for uniform polishing. Additionally, it was expected to give judgment of the

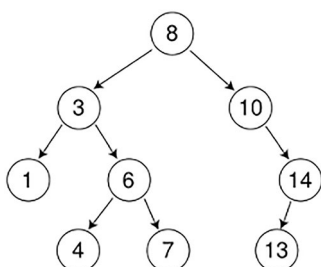


FIGURE 10 | Depth First Search.

TABLE 1 | Apply Depth First Search using stack.

Vertex	8	3	1	6	4	7	10	14
Stack	8	3,10	1,6,10	6,10	4,7,10	7,10	10	14

polishing orientation of the Condyle using the offline programming mode of a robot. Curve Fitting with 53 control points on a single continuous curve. These curve fit points are used for deriving the equation for Robot programming.

4.7 | Mathematical Model of the Artificial Knee

The requirement of curve fitting is for the inverse kinematics calculation of the 6-axis IRB 2400 robot arm. A mathematical model of the artificial knee was made, and a 3D projection tool of the software was used to project the curves on respective planes. All the 3 planes, plane XY, plane ZY, and plane ZX, get a projection view of the corresponding curve. Initially, curves on the patella surface of the knee are considered. A simple polynomial regression method is used in which the control points are coordinated on the curve, and an assumption of curve's nature is a cubic spline curve. Following is the mathematical representation of the respective method.

If a polynomial is represented by an equation as, (Little et al. 2007)

$$y = ax^2 + bx + c \quad (8)$$

Where y is the dependent variable and x is the independent variable. And a, b, c are constants.

For determining the equation of any curve in the form of the equation mentioned above, the values of the constants need to be evaluated. For this reason, the following is the matrix representation of the regression method of curve fitting.

$$\begin{bmatrix} n \sum x^0 & \sum x^0 x^1 & \dots & \sum x^0 x^m \\ \vdots & \vdots & & \vdots \\ \sum x^m & \sum x^m x^1 & \dots & \sum x^m x^m \end{bmatrix} \begin{bmatrix} am \\ \vdots \\ a1 \end{bmatrix} = \begin{bmatrix} \sum yx^0 \\ \vdots \\ \sum yx^m \end{bmatrix} \quad (9)$$

Where n is the number of control points of the curve. For the first iteration, it is assumed that the equation of the curve is a 2-degree equation. Hence above matrix for the case can be written as follows. Hence,

From (8) and (9). The following is obtained

$$\begin{bmatrix} n \sum x^0 & \sum x^0 x^1 & \sum x^0 x^2 \\ \sum x^1 & \sum x^1 x^1 & \sum x^1 x^2 \\ \sum x^2 & \sum x^2 x^1 & \sum x^2 x^2 \end{bmatrix} \begin{bmatrix} c \\ b \\ a \end{bmatrix} = \begin{bmatrix} \sum yx^0 \\ \sum yx^1 \\ \sum yx^2 \end{bmatrix} \quad (10)$$

For comparison between the original values and the curve fit values, 50 control points are plotted by the sung equation obtained from the solution to eliminate the linearity between the points. The constant values a, b, and c are obtained by using these points, and the equation of each curve was calibrated by comparing the Eqn (Arno et al. 2012) of a two-degree polynomial. Table 2 contains coordinate values of control points with respect to the corresponding plane.

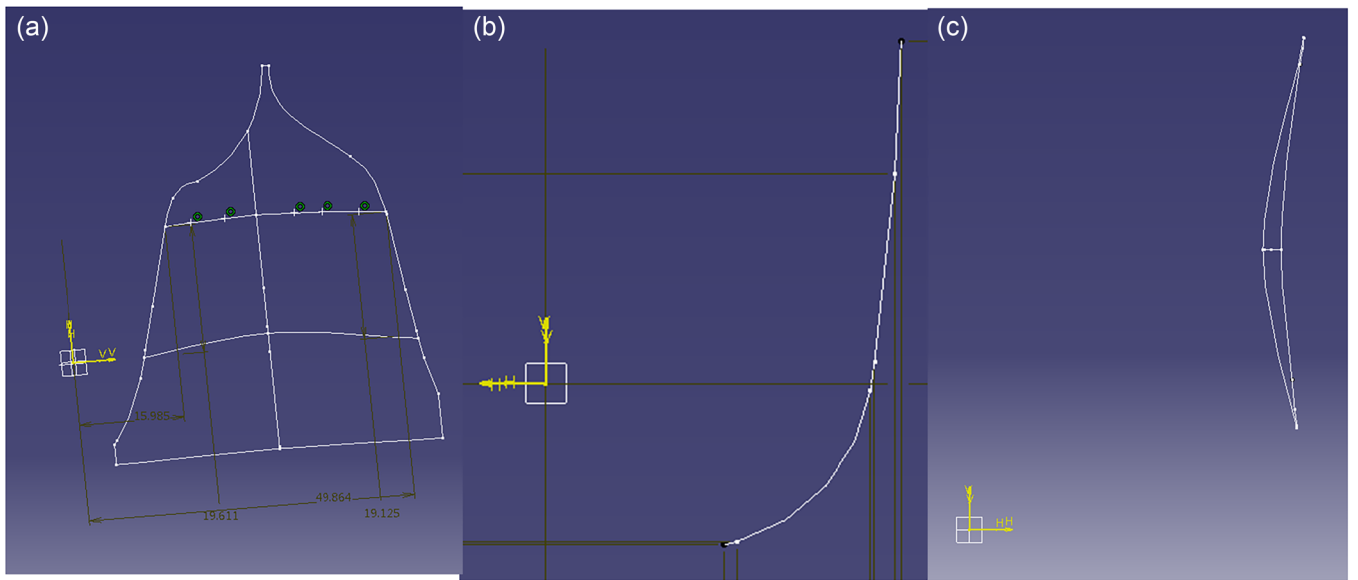


FIGURE 11 | The control points of the femoral Condyle (a) ZY plane (b) XY plane (c) ZX plane. [Color figure can be viewed at wileyonlinelibrary.com]

TABLE 2 | x-y Plane control points.

Sr. no	Plane	Label	X-Coordinate	Y-Coordinate	Y-Curve Fit	a, b, c
1	x-y	1	17.0105	-15.584	-15.44612442	$a = 0.05878411$
			18.268	-15.288	-15.32843101	
			19.992	-14.692	-14.86491982	$b = -1.98022213$
			22.933	-13.177	-13.26770423	
			25.453	-11.238	-11.09015731	$c = 1.22884335$
			27.7	-8.741	-8.51884829	
			29.371	-6.018	-6.22181493	
2	x-y	2	29.371	-6.018	-6.00977924	$a = 1.37306682$
			30.399	-3.488	-3.57179849	
			31.048	-0.729	-0.53823643	$b = -79.69662697$
			31.463	2.077	2.00785196	
			31.878	5.13	5.02689321	$c = 1150.2760175$
			32.339	8.878	8.93506899	
3	x-y	3	32.339	8.878	8.95288984	$a = 3.35740569$
			32.788	13.065	12.88090802	
			33.135	16.851	16.84394818	$b = -209.90939033$
			33.403	20.302	20.45810762	
			33.553	22.555	22.69146738	$c = 3286.00112601$
			33.72	25.532	25.35567896	
4	x-y	4	33.72	25.532	25.53267896	$a = 0.41231053$
			33.87	28.929	28.92990802	$b = -5.22140223$
						$c = -267.21522504$
5	x-y	5	33.87	28.929	28.92899247	$a = 8.52505935e + 01$
			33.949	31.29	31.29002042	$b = -5.7517235e + 03$
			33.995	33.155	33.15498711	$c = 9.70422948e + 04$

Below is the result obtained from the above experimentation and observation. The following graphs were obtained by calculating Equation (1) using Python Programming.

All the curve fit points are plotted as depicted in Figure 12 against the observed value of the x coordinate and hence compared to show the minimum deviation between the observed values and the curve fit values. An irregular variation is observed in xy3. This is due to the consideration of a small domain of control points. The curve fit line satisfies all the points of the observed values and fulfills the desired shape as required on the 3D projection of the ZX plane. The above calculation is made in support of programming a robot in offline mode. The curve fit problem was solved using Python programming to save time and for an optimized outcome in terms of a rough judgment of the surface profile to decide the number of control points for every continuous curve and orientations at points of discontinuity.

4.8 | Coupon Level Polishing

Coupon level polishing, as portrayed in Figure 13 is defined to do polishing manually on the machines (Without a Robot). Such a stage of experiment was required to study the amount of pressure needed to compensate for the vibrations experienced while polishing. In addition to this, it can also give brief conclusions about the layout that should be adopted while polishing. The most important instruction to the polisher is that the polishing should be made orthogonal with respect to the lay of as machined pattern.

4.9 | Vibration Analysis on the End Effector

As shown in the Figure 14 to Varying Excitation Frequencies demonstrates end effector tip deflection across 5 s as the system receives excitation frequencies at 10 Hz, followed by 20 Hz and 30 Hz, and ending with 40 Hz. The figure displays both time on the x-axis and deflection of the tip in millimeters on the y-axis.

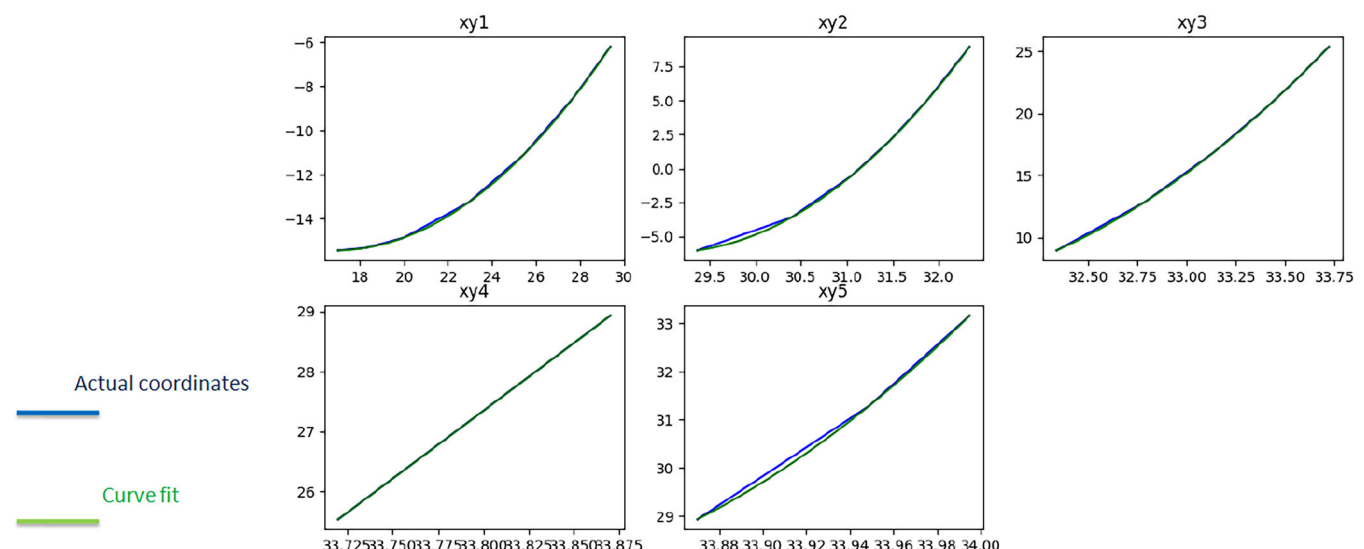


FIGURE 12 | XY plane Curve fit. [Color figure can be viewed at wileyonlinelibrary.com]

When excitation frequencies increase, the vibration cycles shorten while the oscillations intensify throughout each second. The vibration amplitude gets slower with lower frequencies set to 10 Hz and 20 Hz, but it becomes dense and rapid when users apply higher frequencies at 30 Hz and 40 Hz. The increased frequency magnitude does not affect the tip deflection, which stays between ± 0.3 mm, showing good structural stiffness coupled with damping properties. During the measurement period between 2 and 3 s a slight unwanted tremor in oscillation density could indicate that the system approached a resonant condition, particularly when operating at elevated frequencies. The experimental results demonstrate stable vibration amplitudes throughout the frequency test, yet operating at extended frequencies might produce surface defects or micro-patterns during the polishing stage.

The measurement of vibration frequency (Hz) depends on the robot end effector movement speed (mm/s) throughout polishing operations, as shown in Figure 15. The vibration frequency shows a steady upward trend at first when the robot speed rises, since the dynamic behavior remains predictable. The system marks a vital shift at 120 mm/s because the vibration curve demonstrates a brief level region that indicates approaching a resonance condition, which could magnify vibration intensities. The dashed vertical line identifies this speed point, which marks the resonant speed for clarification purposes. After 120 mm/s, the vibration frequency maintains a stable upward pattern. The experimental results demonstrate that running the robot at the near-resonant speed of 120 mm/s might result in amplified machine vibrations, which could affect both the surface quality and introduce abnormalities on finished parts. The optimal performance of the robot requires operating speeds either below 100 mm/s or above 140 mm/s to prevent disturbances from critical resonance.

4.10 | Taguchi Analysis of Robot Polishing

Three different glass abrasive paper surfaces were used to obtain a mirror finish on the flat surface of Co-Cr-Mo alloy

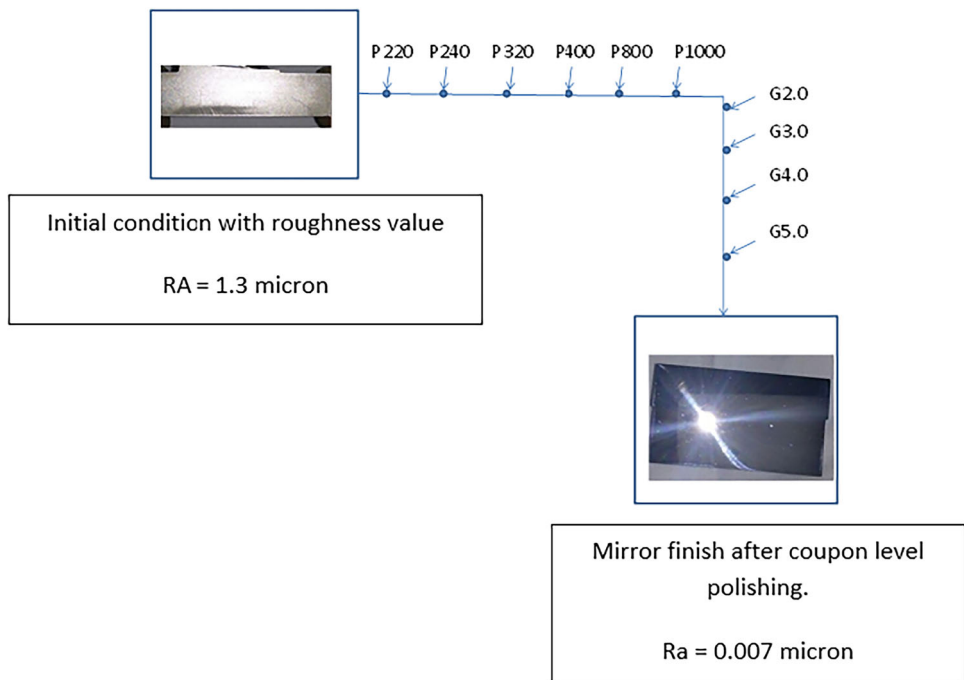


FIGURE 13 | Steps Involved in Coupon Level Polishing. [Color figure can be viewed at wileyonlinelibrary.com]

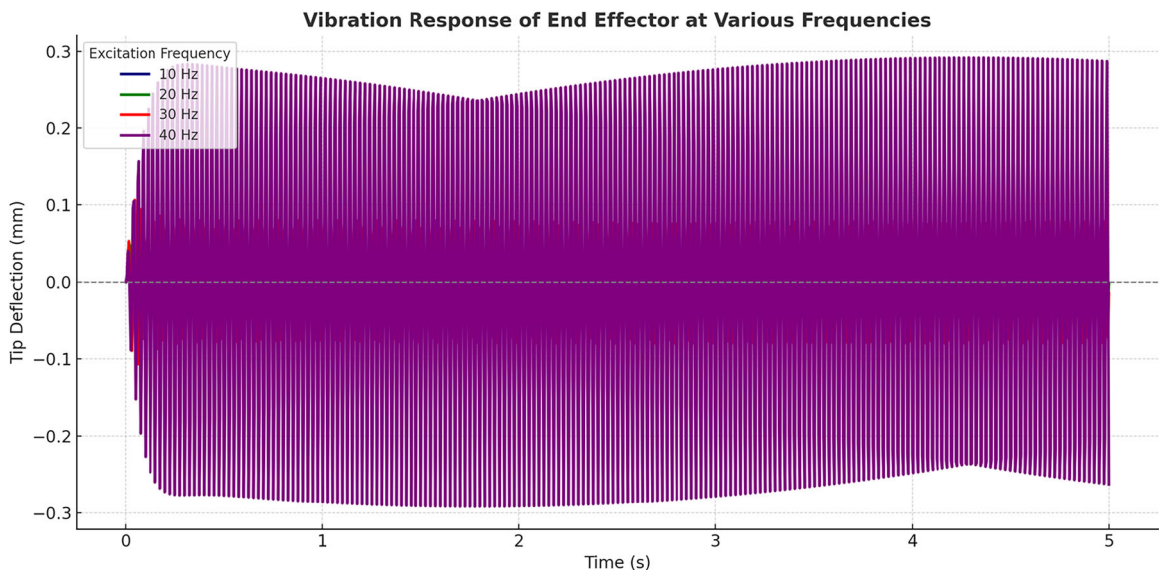


FIGURE 14 | Dynamic Vibration Response of End Effector Subjected to Varying Excitation Frequencies. [Color figure can be viewed at wileyonlinelibrary.com]

Figure 16. These papers are classified according to their abrasive size grading as P220, P800, and 4.0. The rubbing of the surface is done manually. For each paper, the work piece needs to be rotated 90 degrees consecutively. Shear force is needed while removing the material from the surface. If not rotated 90 degrees, the next step will be having tensile force dominance or irregular shear. Hence, for each step, the work piece needs to be rotated 90 degrees.

After the above observation, as portrayed in Table 3 it was concluded that manual polishing is not enough to generate a threshold amount of shear force for material removal for mirror

finish polish scale. After using P220 and G4.0, the roughness value increases by 0.01 to 0.015 microns compared to its predecessor. For improving the surface profile of the material, the surface should be treated using some other abrasive slurry, like diamond slurry, which was made available on cloth polishing. The following are the results of stage-wise observations of flat surface polishing. Figure 14 portrayed the relative variations of Ra and Rz values for different grades of polishing papers.

The objective is to minimize the surface roughness of Co-Cr-Mo alloy. Therefore, the “smaller the better” approach is used to reduce the surface roughness being studied.

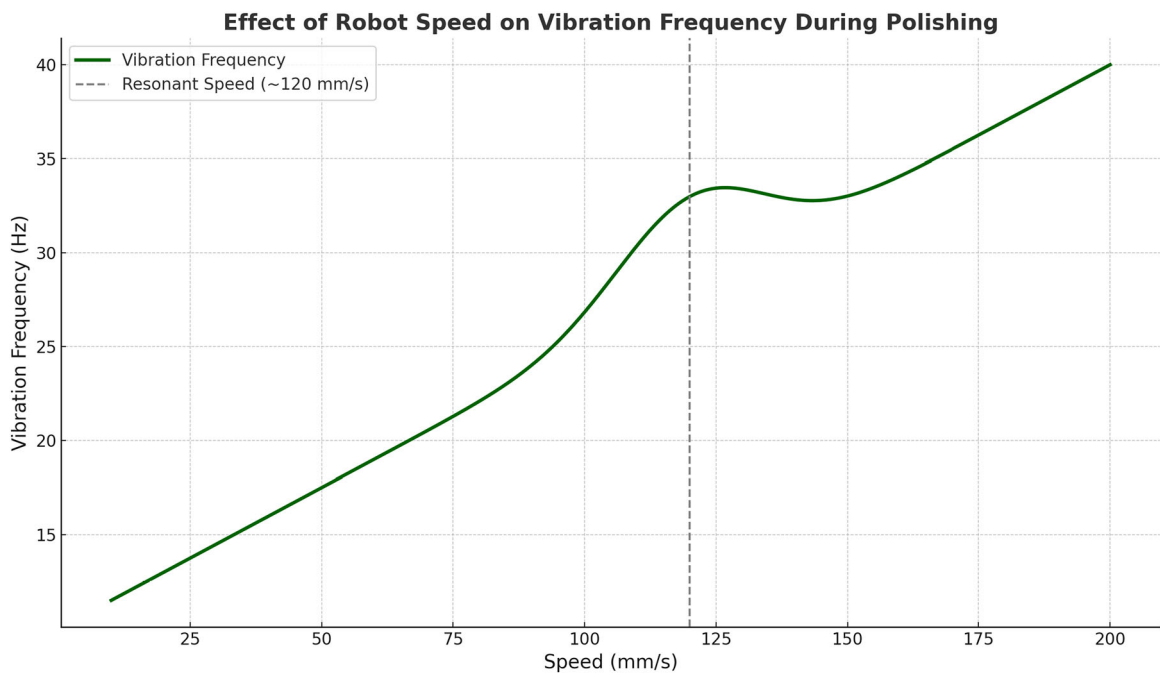


FIGURE 15 | Effect of Robot Speed on Vibration Frequency during Polishing. [Color figure can be viewed at wileyonlinelibrary.com]

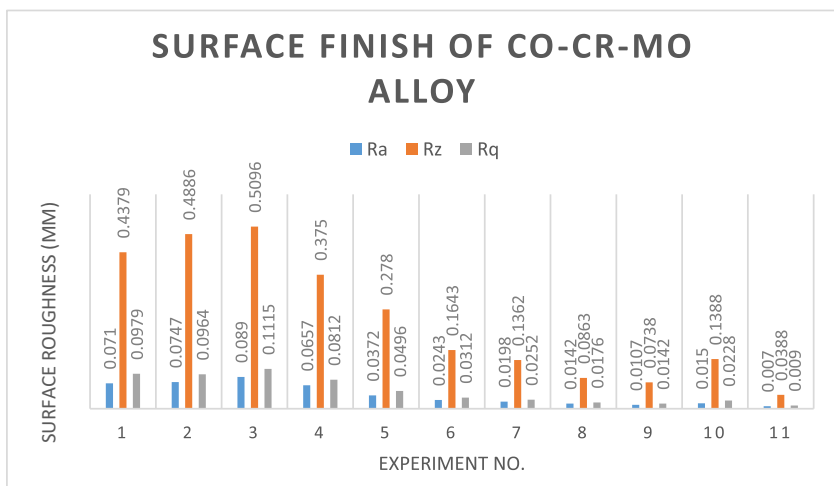


FIGURE 16 | Surface roughness values of polishing Co-Cr alloy. [Color figure can be viewed at wileyonlinelibrary.com]

TABLE 3 | Coupon level polishing the Co-Cr-Mo alloy surface roughness.

Ex. No.	Grade Paper	Time (min)	Strokes /min	Stroke length (cm)	Ra (μm)	Rz	Rq
1	P220	30	100	15	0.071	0.4379	0.0979
2	P220	45	125	17	0.0747	0.4886	0.0964
3	P220	60	150	19	0.089	0.5096	0.1115
4	P800	30	125	19	0.0657	0.3750	0.0812
5	P800	45	150	15	0.0372	0.2780	0.0496
6	P800	60	100	17	0.0243	0.1643	0.0312
7	G4.0	30	150	19	0.0198	0.1362	0.0252
8	G4.0	45	100	17	0.0142	0.0863	0.0176
9	G4.0	60	125	15	0.0107	0.0738	0.0142

$$\eta = -10 \log 10 (y^2) \quad (11)$$

Where η = efficiency of the Robot system and y = Surface roughness

As depicted in Figure 17(a-d), the main effect plot highlights the individual impact of each control factor at different levels. Through the Taguchi method, the optimal control factors are determined as Grade paper 4.0, a polishing time of 60 s, a stroke speed of 100 strokes per minute, and a stroke length of 15 cm. The predicted optimal surface roughness is 0.00519 μm , compared to the experimentally achieved value of 0.00741 μm during robotic polishing. This outcome underscores the effectiveness of the Taguchi method in identifying ideal process parameters for robot-assisted polishing of Co-Cr-Mo alloy.

In the Taguchi analysis for polishing Co-Cr-Mo alloy, the main effect plot serves as an essential tool to evaluate the impact of various process parameters—such as surface roughness, material removal rate, and polishing efficiency—on the response variables. During polishing Demircioglu (2017) using an Industrial IRB 2400 Robot, parameters like stroke speed, polishing time, abrasive type, and stroke length significantly influence the results. The main effect plot is created by averaging the response values at each factor level, disregarding the effects of other variables. A steep slope in the plot suggests a strong influence of the factor on the polishing outcome, whereas a nearly horizontal line indicates minimal or no effect. Stroke length, for instance, impacts the uniformity and consistency of the polishing process, and the main effect plot helps

determine whether adjusting the stroke length enhances surface quality.

4.11 | Regression Model of Surface Roughness of Co-Cr-Mo Alloy

The regression model shown in Figure 18 analyses the relationship between the independent variables—stroke speed, polishing time, abrasive type, and stroke length—and the dependent variable, surface roughness. The model demonstrates how variations in these independent factors influence the dependent outcome. By employing a four-variable equation, it seeks to identify the optimal plane that minimizes discrepancies between the model's predictions and the actual experimental data. The model's performance is evaluated using the adjusted R^2 value from the training data, reflecting its ability to fit the data with minimal error. As a supervised learning method, regression identifies correlations between variables, as expressed in Eqn (Zhenyu and Jukka Pajarin 2015), and supports the prediction of continuous outcomes based on one or more predictors. This approach estimates the relationships between the target variable and the predictors, uncovering data trends and enabling accurate predictions of continuous values. The surface roughness predictions for the Co-Cr-Mo alloy showed only a 5% error between experimental results and the regression model's estimates.

$$\begin{aligned} \text{Surface Roughness Ra } (\mu\text{m}) = & -0.130 + 0.000001\text{GrP} \\ & - 0.000590T + 0.000243S \\ & + 0.01032SL \end{aligned} \quad (12)$$

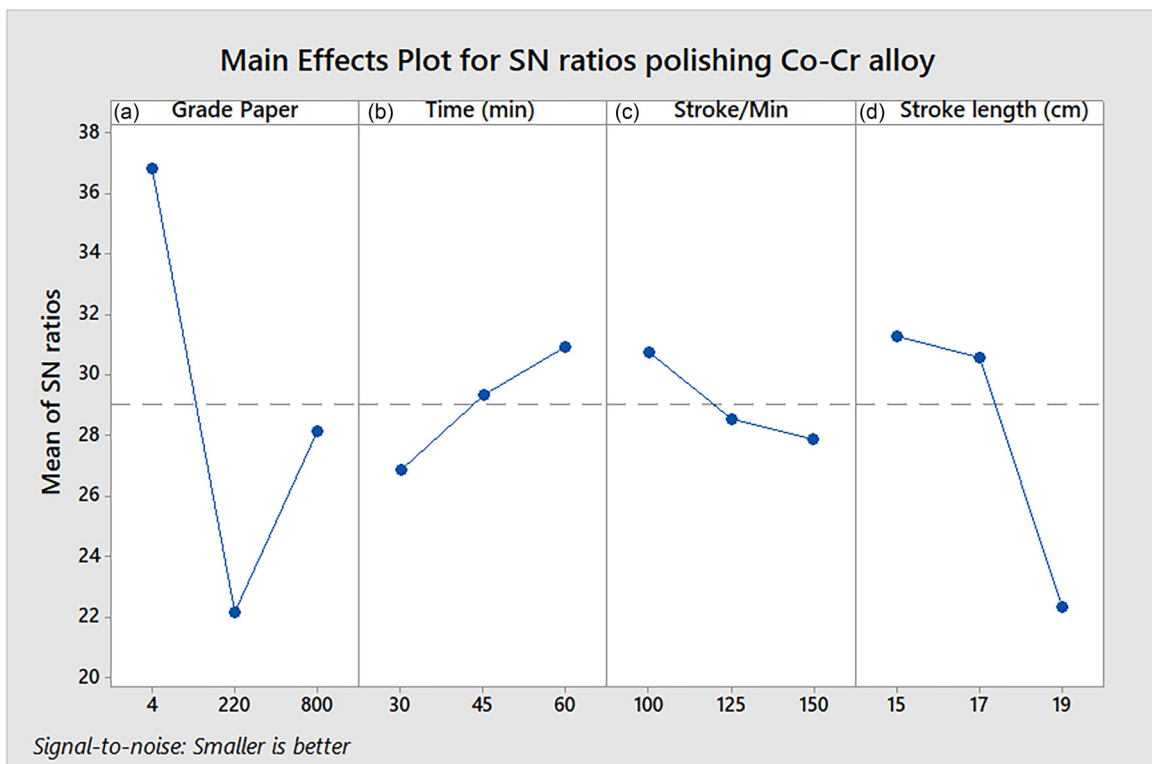


FIGURE 17 | Main effect plot for Surface roughness of Co-Cr-Mo Alloy (a) Grade paper (b) Time (min) (c) Stroke/min (d) Stroke length (cm). [Color figure can be viewed at wileyonlinelibrary.com]

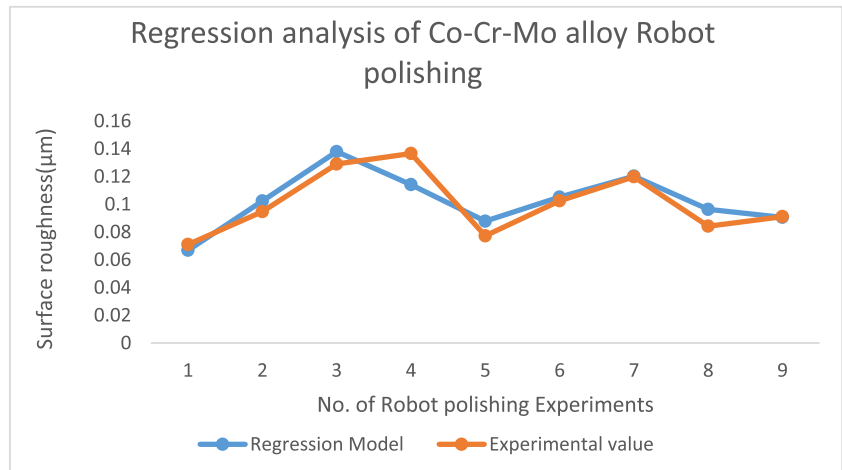


FIGURE 18 | Regression model analysis of Co-Cr-Mo alloy polishing. [Color figure can be viewed at wileyonlinelibrary.com]

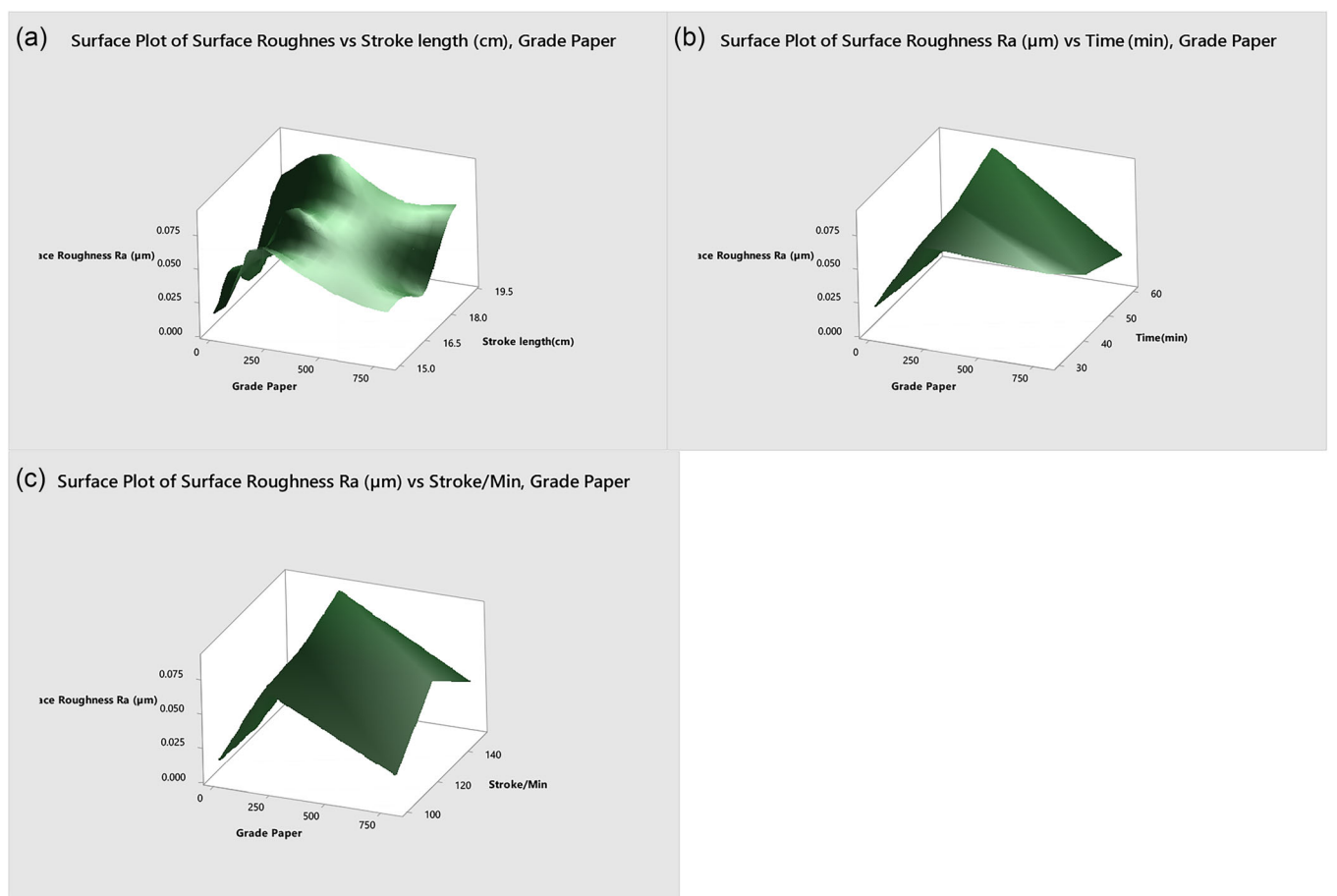


FIGURE 19 | 3D Surface plot of Surface roughness with Co-Cr-Mo robot polishing (a) Grade paper and Stroke length (b) Grade paper and Time (c) Grade paper and stroke. [Color figure can be viewed at wileyonlinelibrary.com]

The 3D surface plot illustrated in Figure 19 provides a graphical tool to explore the relationships among three variables. In the context of analyzing the performance of cobalt-chromium-molybdenum (Co-Cr-Mo) alloy polishing with the Industrial IRB 2400 Robot, these plots offer insights into how various process parameters impact surface roughness (Ra). As shown in Figure 17(a), the plot highlights the variation in surface roughness with different abrasive grade papers and stroke lengths during robotic polishing. Typically,

finer abrasive grades result in smoother surfaces, while changes in stroke length can either enhance surface uniformity or compromise it if excessive length causes uneven force distribution. Figure 17(b) demonstrates the relationship between abrasive grade and polishing time on surface roughness. Prolonged polishing generally produces a smoother surface due to greater material removal; however, over-polishing can negatively affect the surface through increased heat or abrasive wear. Lastly, Figure 17(c)

investigates the combined impact of abrasive grade and stroke motion/pattern on surface roughness. The stroke pattern—whether linear, circular, or oscillatory—plays a critical role in achieving polishing uniformity. Optimizing the interplay between abrasive grade and stroke motion is essential for achieving the desired surface finish.

For verification of the Co-Cr surface treatment of same methodology, a flat piece of Co-Cr material was taken and treated in two stages. 1st treated with Trizact A16 belt with 1500 rpm of grinding wheel feed and at the next stage with A6 Trizact belt. Results are shown below.

Figure 20 portrayed the different polished surfaces of different Co-Cr material samples. Below shown is the roughness calculation by taking the evaluation length of 12.5 mm. The results were obtained with 2-stage polishing of the flat Co-Cr Condyle. The next section is the trial on the available SS Condyle patella surface on unbounded wheels, which then includes 4 steps into the main process.

4.12 | Femoral Condyle SS-304 In 4 Steps

Primarily, surface 9 of the SS Condyle (patella surface) is taken for the unbounded wheel trials. The polishing pattern and the lay pattern are orthogonal to the machining lay pattern. With that dedicated way of polishing following are the results which were as desired results of surface finish. This finishing is obtained by applying diamond slurry of 2–4 grades at the 3rd stage of polishing as mentioned in Figure 21.

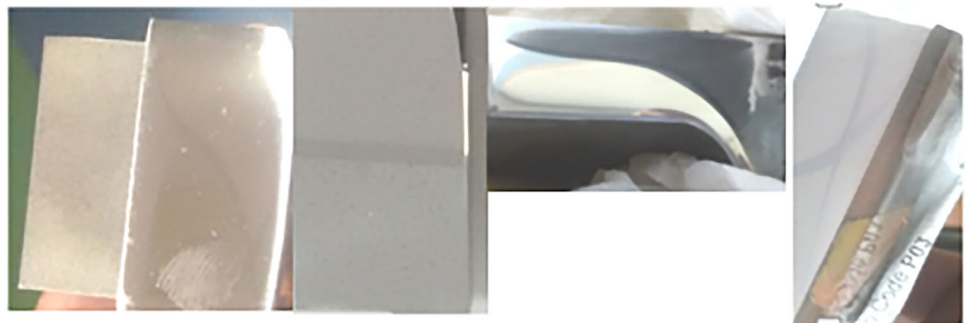


FIGURE 20 | Surface Finish on Co-Cr Flat Piece. [Color figure can be viewed at wileyonlinelibrary.com]



FIGURE 21 | Surface Finish of SS 304 Femoral Condyle with three different views. [Color figure can be viewed at wileyonlinelibrary.com]

The Figure 22 depicts the measurement of the polished patella surface with an evaluation length of 12.5 mm orthogonal to the buffing lay pattern. Uniformity after 4th stage is seen on the surface comparatively. According to observations in 4.2 and 4.3 sections, which are treated with polishing level 2 steps and 4 steps respectively, 2 steps that involve Trizact A16 and A6 belts are only able to make the surface reach 0.061 µm to 0.067 µm. According to ISO standards of surface grade, the surface fits in grade N6. The required grade should be N3, N2. The addition of 2 unbounded wheels can make the surface till the required super finish scale. After observation, the involvement of the 4-step polishing is decided and to be included in the RFC for polishing FC of Co-Cr using a robot. For obtaining uniform polishing, the repeatability in the feed of abrasive to all the pressure points should have the least error. If done manually, the repeatability will have a maximum error of greater than 8000 microns, while using a robot can overcome this problem. The robot used for polishing the Condyle is IRB2400, which has a dynamic repeatability of 60 microns. Hence, for polishing purpose, a robot is used rather than a manual type of polishing.

4.13 | Robot Programming for Polishing the Co-Cr Condyle

The above-explained polishing sub-divisions of the surfaces are classified into different subroutines in the RAPID program of the Robot. Subroutine is defined as a non-active routine of a program that contains the Pose of TCP for different coordinate points of a frame of reference and could be activated by calling it into the main program using the

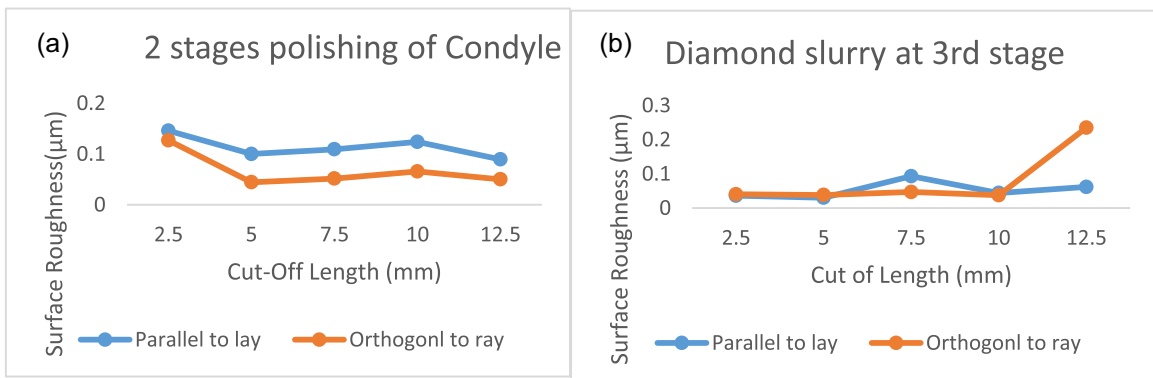


FIGURE 22 | Condyle polishing of (a) 2 Stage (b) Diamond Slurry at 3rd stage. [Color figure can be viewed at wileyonlinelibrary.com]

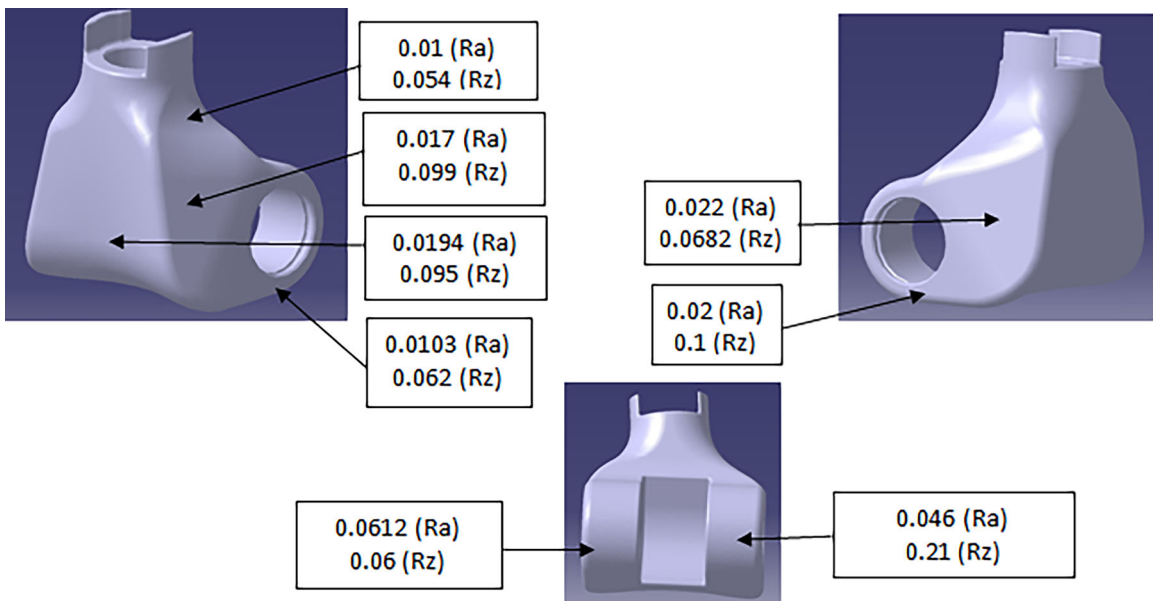


FIGURE 23 | Different surface roughness values of Co-Cr Condyle. [Color figure can be viewed at wileyonlinelibrary.com]

ProCall function in the RAPID programming language. Each of the sub-divisions is been programmed in one subroutine for all 4 machines. Hence, the total number of subroutines required to program the polishing surface code is 64. More 2 subroutines were made to program the Home position of TCP and 4 subroutines for orthogonal polishing of the polishing machine w.r.t the machining lay. Hence, a total of 70 subroutines are made to program the code. The total cycle time of the robot is defined as the time required to complete 1 cycle of the main programmed code. For the Program made of polishing the Condyle, the total cycle time comes out to be 60 min in polishing on all 4 machines with repeating cycles for one surface in incremental behavior for each machine step. For effective polishing, a FOR loop in the program repeats the subroutine for each surface 5, 10, 25, 25 times on a16, a6, unbounded1, and unbounded2 polishing stations, respectively. Co-Cr Condyle was polished, attempting all surfaces using the IRB 2400 robot, and 90% of the surfaces were polished will N2 (Super-Finishing towards Lay). Following (Figure 23) are the roughness parameters after multiple attempts on surface 9 (Patella Surface).

4.14 | Robot Polishing of Co-Cr Alloy

The desirable value of N2 grade of super finishing on a large size Condyle has been polished on a 4-station Robot finishing cell programmed on IRB 2400 with a total cycle time of 50 min. It's not always repeatable to define a fixed set of control points while online programming the robot, but the pattern of polishing is fixed, and thus though there is variability in control points, it seems that be polishing results are unchanged with small variability in the control points of the robot. The measurements are on the different surfaces of the Condyle, named as Patella surface, Articulating surfaces, and side surfaces with Lay parallel and Lay orthogonal reading as portrayed in Figure 24. The conclusion on the result is that the surface finish is obtained as desired, but to obtain more optimized uniformity, a larger number of control points needs to be addressed during the programming of the robot. This increase in the number of control points is a bit difficult to manipulate in manual type programming. Hence, for the desired result, the program needed to be made an add-on to the user interface, which can calculate a larger number of control points is less time.



FIGURE 24 | Robot polished components of Condyle. [Color figure can be viewed at wileyonlinelibrary.com]



FIGURE 25 | Trizact belt Abrasive, Active reducing height after incremental use. [Color figure can be viewed at wileyonlinelibrary.com]

4.15 | Polishing Belts

After experimentation with coupon-level polishing, it was known how many numbers of steps and strokes are required to polish a Co-Cr material workpiece. In reference to that data, polishing belts was a crucial job. Some aspects are very important to know about the polishing belts. The polishing belts should be long-lasting, and the number of abrasive particles on the belts should be sufficient to polish the workpiece at least once. These aspects can affect the total cycle time of the robot and, hence, finally have an effect on the production of the component. For minimizing these two things, the belts that are to be selected are considered as the number of polishing stations in the robot finishing cell. After different experimentations, abrasive belts of the same properties but two different grades were selected. The literature review for the polishing operation is mainly focused on the belt selection for polishing different materials of different shapes. The main problem faced during polishing is degradation of the belt abrasive due to material removal of the workpiece after using it several times. The thickness of the belt or the abrasive grade on it gets poorer after multiple uses. To overcome this problem, Trizact belts are found to be best suited for the respective operation. Trizact belt technology has been patented by 3 M Technology with different belt mineral geometry as compared to conventional polishing belts as portrayed in Figure 25.

Unlike conventional belts, Trizact shape and geometry is 3 3-dimensional pyramidal-like geometry which has abrasive minerals at each consecutive layer. After multiple uses of the belt, the sharpness remains almost the same to cover more surface area of been polished surface. According to (Patent US 20050060947 A1. 2015), a combination of large topological composites with large ceramic abrasives together makes an abrasive article. The abrasive composite forming abrasive article has a height of at least 500 microns, and the abrasive particle in the composite has an average particle size of 40 microns.

The SEM results are shown in Figure 26, which has morphological data of Trizact belts, indicating the size of the abrasive active along its length to be 500 microns. For standardization of these belts according to European standards, A6 is P1200 grade and A16 is P2500 grade abrasive belts. The abrasive particles are of aluminum dioxide (Patent US 20050060947 A1. 2015). According to these standards, the abrasive particle roughness is 0.11 and 0.025 microns, respectively. Hence, due to this property of the belt, they were selected for the superfinishing polishing operation of the Co-Cr-Mo femoral Condyle. The abrasive particle size of 3 M abrasive belts is between 0.3 microns to 0.053 microns, corresponding to A6 to A16 (Patent US 20050060947 A1. 2015). Premium SiC abrasive belts have irregular morphology of abrasive distributions. That can increase the rate of wear of the abrasive. Trizact belts have abrasive actives, and it has abrasive particles. Hence, after every stroke, a new abrasive particle is used for polishing. Hence, the Trizact belt was a wise choice for the desired polishing.

5 | Conclusions

A few polishing trials were made on a flat piece of Co-Cr material flat piece. After obtaining the results on the flat pieces, the same POC was implemented on an SS-304 FC in coupon-level polishing. The result obtained helped to conclude that 2 more steps of polishing are required, which included compressing cotton cotton-unbounded wheel with a diamond abrasive slurry. The results obtained in coupon-level polishing in 4 steps were promising and desirable.

1. The same POC was implemented on robot path planning for polishing FC using IRB 2400 SM in the designed RFC. For the effective operation, primarily the path planning was virtually simulated in RS and concluded the free space for the robot arm in RFC. RFC was designed, which includes 4 grinding machines with rigid positions. The machines are equipped with abrasive belts of Trizact A16, A6, and 2 compressed cotton unbounded wheels.

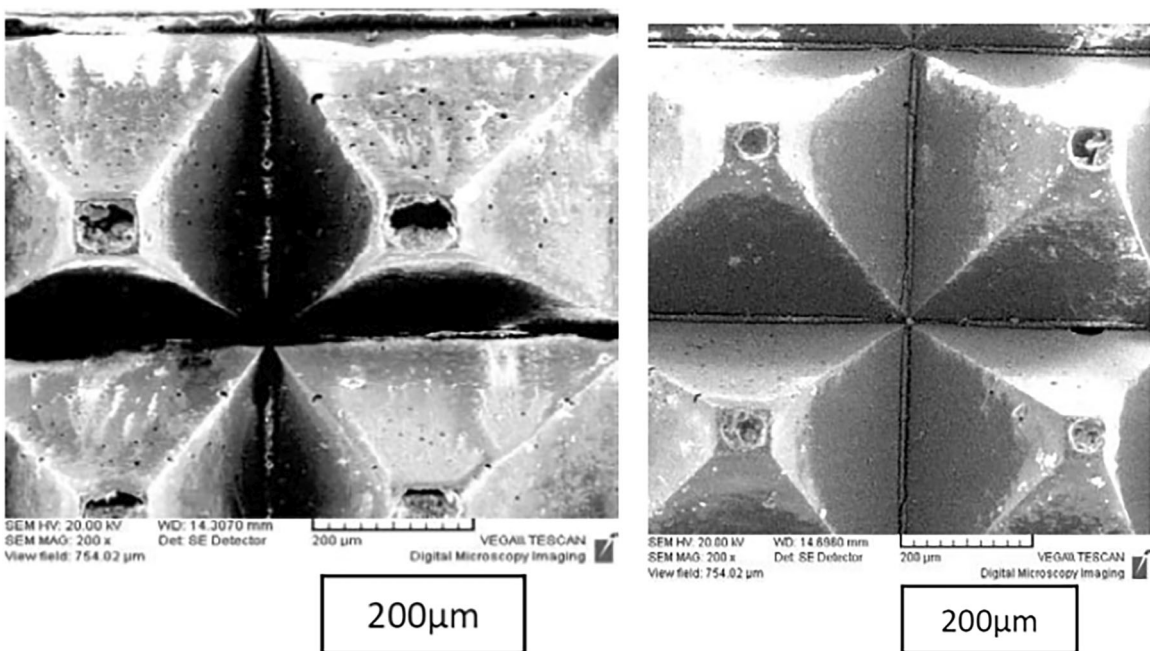


FIGURE 26 | SEM image of Trizact belts.

2. A fixture for FC to get a hold on SM was designed using SS 304 material and with a self-holding Mohr's taper. An analysis was made, and the design was approved as a safe design. To study the path planning FC, surface 9 of FC was considered, and using CATIA, a 2D projection was made concerning all three orthogonal planes to study the continuity of the curves present on the surface. The curve fit method was used to determine the curve equation within the domain of continuity. This can help to decide the number of control points needed to fit the curve and hence the path for the robot.
3. Online programming was done on SM by path planning, as concluded in a virtual simulation. The result of the surface roughness on FC was desirable, but the surface uniformity was disturbed due to multiple trials of programming on the same FC. As a result, the same POC will be examined on a Co-Cr FC in RFC. Sequential experimentation results are shown, and using a justified algorithm, desirable results were obtained.
4. According to Rosler's Report on Super finishing on Orthopedic implants and medical instruments [25], the results obtained on polishing the knee using a drag finishing machine come out to be $R_a = 0.2$ microns and $R_z = 0.16$ microns in 3-stage abrasive bucket polishing. The obtained results were way better than the existing method results, as $R_a = 0.008$ microns and $R_z = 0.05$ microns. This method consists of 4 stages, but it is cost-effective than Rosler's polishing method.

Ethics Statement

The authors have nothing to report.

Conflicts of Interest

The authors declare no conflicts of interest.

Consent to Participate

The authors have nothing to report.

Consent to Publish

The authors have nothing to report.

Data Availability Statement

Data sharing is not applicable to this article as no new data were created or analyzed in this study.

References

- Arno, S., J. Fetto, Q. Nguyen, et al. 2012. "Evaluation of Femoral Strains With Cementless Proximal-Fill Femoral Implants of Carried Stem Length." *J. of Clinical Biomechanics* 27, no. 7: 680–685.
- Arun, K. V., and K. K. Jadhav. 2016. "Behaviour of Human Femur Bone Under Bending and Impact Loads." *European Journal of Clinical and Biomedical Sciences* 2, no. 2: 6–13. <https://doi.org/10.11648/ejcbs.20160202.11>.
- Brunetter, D. M., P. Tengvall, M. Textor, and P. Thomsen. 2001. "Titanium in Medicine." In *Material science surface science engineering biological responses and medical applications*, Springer.
- Buford, A., and T. Goswami. 2004. "Review of Wear Mechanisms in Hip Implants: Paper I- General." *Materials & Design* 25, no. 5: 385–393, August.
- Byran, R., P. B. Nair, and M. Taylor. 2012. "Influence of Femur Size and Morphology on Load Transfer in the Resurfaced Femoral Head: A Large Scale, Multi-Subject Finite Element Study." *Journal of Biomechanics* 45, no. Issue 11: 1952–1958.
- Crocklarell, Jr MD., J., M. Hicks John, Schroeder Jason, et al. 2010. "Total Knee Arthroplasty With Asymmetric Femoral Condyles and Tibial Tray." *Journal of Arthroplasty* 25, no. 1: 108–113.
- Demircioglu, P. 2017. "3.17 Topological Evaluation of Surface in Relation to Surface Finish." *Journal Comprehensive Materials Finishing*.
- Ducheyne, P., L. Heymans, M. Martens, E. Aernoudt, P. de Meester, and J. C. Mulier. 1977. "The Mechanical Behaviour of Intracondylar Cancellous Bone of the Femur At Different Loadings Rates." *Journal of Biomechanics* 10, no. Issues 11–12: 747–762.
- Ebrahim, H., M. rabinovich, V. Vuleta, et al. 2012. "Biomechanical Properties of An Intact, Injured Repaired and Healed Femur: An

- Experimental and Computational Study." *Journal of Mechanical Behavior of Biomedical Materials* 16: 121–135.
- Gregory, W., B. Kubacki, L. Jeremy, and Gibert. 2017. "Electro Surgery Induced Damaged to Ti-6Al-4V and Co-Cr-Mo Alloy Surfaces in Orthopaedic Implants In Vivo and Vitro." *Journal of Arthroplasty* 32, no. 11: 3533–3538. <https://doi.org/10.1016/j.arth.2017.06.015>.
- Hallab, N. J. 2017. "7.7 Fretting Corrosion of Orthopaedic Implants." *Journal of Comprehensive Biomaterials II* 7: 106–117. <https://doi.org/10.1016/b978-0-12-803581-8.10176-6>.
- Jones, L. C., L. D. Timmie, Topolesic, and A. K. Tsao. 2017. "Biometrials in Orthopaedic Implants." In *Mechanical Testing on Orthopaedic Implants*. Elsevier. <https://doi.org/10.1016/B978-0-08-100286-5.00002-0>.
- Kandlikar, S. G., D. Schmitt, A. L. Carrano, and J. B. Taylor. 2005. "Characterization of Surface Roughness Effects on Pressure Drop in Singlephase Flow in Minichannels." *Physics of Fluids* 17, no. 10: 100606. <https://doi.org/10.1063/1.1896985>.
- Little, J. P., F. Taddei, M. Viceconti, Dw Murray, and H. S. Gill. 2007. "Changes in Femur Stress After Hip Resurfacing Arthroplasty: Response to Cytological Loads." *Journal of Clinical Biomechanics* 22, no. 4: 440–448.
- Patent US 20050060947 A1. "Composition for abrasive articles" published on 24th March 2015.
- Tigani, D., M. Fosco, R. Ben Ayad, and R. fantasia. 2013. "Orthopaedic Implant Materials and Design." *Wear of Orthopaedic Implants and Artificial Joints, A Volume in Wood head Publishing Series in Biomaterials*: 133–177.
- Zaman, H. A., S. Sharif, D. W. Kim, M. H. Idris, M. A. Suhami, and Z. Tumurkhuyag. 2017. "Machinability of Cobalt-Based and Cobalt Chromium Molybdenum Alloys - A Review." *Procedia Manufacturing* 11: 563–570. <https://doi.org/10.1016/j.promfg.2017.07.150>.
- Zhenyu, Y., L. T.-h, and T. S. Jukka Pajarinen. 2015. "Stuart Goodman, "Chapter 12- Host Response to Orthopeadic Implants Metals and Plastics)." *Host Response to Biomaterials*: 315–373.

Appendix A

Forward kinematics of IRB2400

```

clc;
clear all;
close all;
format short;
theta4 = 0; theta5 = 0.3790; theta6 = 0; theta1 = 0; theta2 = 0.0863;
theta3 = -0.5023;

d1 = 615; d2 = 0; d3 = 0; d4 = 755; d5 = 0; d6 = 0;
a1 = 0; a2 = 840; a3 = 0; a4 = 0; a5 = 0; ax6 = 0;
alpha1 = -pi/2; alpha2 = 0; alpha3 = -pi/2; alpha4 = pi/2; alpha5 = -pi/2;
alpha6 = 0;

t4 = [cos(theta4) -sin(theta4)*cos(alpha4) sin(theta4)*sin(alpha4) a3*cos(theta4);
       sin(theta4) cos(theta4)*cos(alpha4) -cos(theta4)*sin(alpha4) a4*sin(theta4);
       0 sin(alpha4) cos(alpha4) d4;
       0 0 0 1];

t5 = [cos(theta5) -sin(theta5)*cos(alpha5) sin(theta5)*sin(alpha5) a3*cos(theta5);
       sin(theta5) cos(theta5)*cos(alpha5) -cos(theta5)*sin(alpha5) a5*sin(theta5);
       0 sin(alpha5) cos(alpha5) d5;
       0 0 0 1];

t6 = [cos(theta6) -sin(theta6)*cos(alpha6) sin(theta6)*sin(alpha6) a3*cos(theta6);
       sin(theta6) cos(theta6)*cos(alpha6) -cos(theta6)*sin(alpha6) ax6*sin(theta6);
       0 sin(alpha6) cos(alpha6) d6;
       0 0 0 1];
%
% H = t1*t2*t3*t4*t5*t6

t1 = [cos(theta1) -sin(theta1)*cos(alpha1) sin(theta1)*sin(alpha1) a1*cos(theta1);
       sin(theta1) cos(theta1)*cos(alpha1) -cos(theta1)*sin(alpha1) a1*sin(theta1);
       0 sin(alpha1) cos(alpha1) d1;
       0 0 0 1];

t2 = [cos(theta2) -sin(theta2)*cos(alpha2) sin(theta2)*sin(alpha2) a2*cos(theta2);
       sin(theta2) cos(theta2)*cos(alpha2) -cos(theta2)*sin(alpha2) a2*sin(theta2);
       0 sin(alpha2) cos(alpha2) d2;
       0 0 0 1];

t3 = [cos(theta3) -sin(theta3)*cos(alpha3) sin(theta3)*sin(alpha3) a3*cos(theta3);
       sin(theta3) cos(theta3)*cos(alpha3) -cos(theta3)*sin(alpha3) a3*sin(theta3);
       0 sin(alpha3) cos(alpha3) d3;
       0 0 0 1];
%
q = [theta1 theta2 theta3 theta4 theta5 theta6]
L(1) = Link([theta1,d1,a1, alpha1]);
L(2) = Link([theta2,d2,a2, alpha2]);
L(3) = Link([theta3,d3,a3, alpha3]);
L(4) = Link([theta4,d4,a4, alpha4]);
L(5) = Link([theta5,d5,a5, alpha5]);
L(6) = Link([theta6,d6, ax6, alpha6]);
rob = SerialLink(L)
qw = rob.fkine(q)
rob.plot(q)
H = t1*t2*t3*t4*t5*t6

```